Oscillation of Acceleration Accompanying Shear Band and Subsequent Time-Dependent Behavior in Overconsolidated Clay under Undrained Plane-Strain Conditions

Oscillation de l'accélération accompagnant la formation de bandes de cisaillement et comportement dépendant du temps dans une argile surconsolidée en déformations planes et conditions non drainées.

Noda T.
International Member, Nagoya University, Japan

Xu B.
Student Member, Nagoya University, Japan

ABSTRACT: In this paper, a compression test on a rectangular overconsolidated clay specimen under plane strain, constant cell pressure, and undrained conditions was simulated using a soil-water coupled finite deformation analysis code taking inertial loads into consideration, and the following results were obtained: 1) In order to reproduce uniform deformation in a perfect specimen with no initial geometric imperfection, it is necessary to have conditions in which the "permeability coefficient is zero" so that pore water migration does not virtually occur, as well as to apply an initial distribution of velocity, acceleration and pore water pressure to the interior as well as the boundary in accordance with the vertical velocity of the top/bottom ends so as to satisfy the undrained conditions; 2) In specimens with initial geometric imperfection set to a very small amplitude primary cosine curve, when a vertically symmetric vertical displacement was applied under displacement control from static conditions, shear banding occurred in the specimen, and accelerations were generated from that part; 3) After the load became unstable, by changing to load control and maintaining the load constant, creep behavior under undrained conditions was exhibited by the specimen.

RÉSUMÉ: Un essai de compression sur une éprouvette rectangulaire d'argile surconsolidée, en déformations planes et conditions non drainées est modélisé en utilisant une analyse couplée en grandes déformations, prenant en compte les forces d'inertie. Cette analyse a apporté les résultats suivants: 1) En vue de reproduire une déformation uniforme dans une éprouvette parfaite sans défaut géométrique initial, il est nécessaire d'avoir des conditions dans lesquelles le « coefficient de perméabilité est égal à zéro » de telle sorte qu'il n'y a aucun écoulement d'eau, ainsi que d'appliquer une distribution initiale de vitesses, d'accélérations et de pressions interstitielles à l'intérieur ainsi qu'aux limites de l'éprouvette en accord avec la vitesse verticale de la base et du haut de celle-ci en vue de satisfaire les conditions de non drainage ; 2) Pour des éprouvettes présentant un défaut géométrique initial de très faible amplitude, quand un déplacement vertical symétrique est appliqué à déplacement contrôlé, des bandes de cisaillement se développent dans l'éprouvette et des accélérations se développent à partir de là ; 3) Après que le chargement soit devenu instable, en changeant pour un chargement contrôlé en effort et en maintenant l'effort constant, l'éprouvette présente un comportement de fluage en conditions non drainées..

KEYWORDS: imperfection, shear band, acceleration oscillation.

MOTS CLES : imperfection, bande de cisaillement, oscillation de l'accélération

1 INTRODUCTION

In bifurcation analysis or shear strain localization analysis of soil specimens, calculations are normally carried out on a uniform deformation field assuming quasi-static conditions that ignore the effect of inertia forces (Ikeda et al. 2003, Wan et al. 1990). The authors have developed the GEOASIA code, which is capable of performing analyses without distinction dynamic/static problems, extending the static soil-water coupled finite deformation analysis that has been carried out to date (Asaoka et al. 2007, Noda et al. 2008). In this paper, the strain localization problem of rectangular specimens of saturated overconsolidated clay under undrained and constant side pressure conditions was addressed, checking the conventional solutions that were obtained under quasi-static assumptions and taking the problem to be a dynamic problem that considers inertial term. This paper introduces several phenomena such as the generation of accelerations and time-dependent behavior (creep) associated with the occurrence of shear banding as newly found calculation results using GEOASIA.

2 CALCULATION CONDITIONS

Fig. 1 shows the finite element mesh and boundary conditions used in the calculations. The calculation assumed 2-dimensional plane strain conditions and a saturated rectangular specimen with 3.5 cm wide and 8 cm high in the isotropic consolidation state. The specimen was a fully remolded overcolsolidated clay. As the elasto-plastic constitutive model in the analysis, the SYS Cam-clay model (Asaoka et al. 2002), the degree of structure was R^*=1.0 and there was no effect of the initial anisotropy and induced anisotropy (ζ_0=0, br=0).

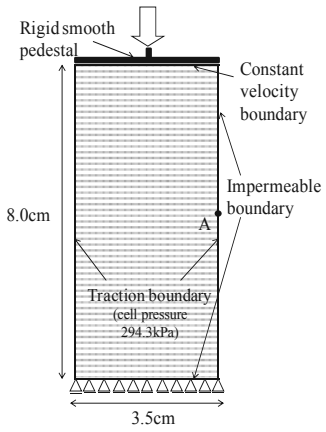

Fig. 1 Finite element mesh and boundary conditions

Table 1 shows the soil elasto-plastic constants and the set of initial values used in the calculations. Apart from the

overconsolidation degradation index m, which controls the overconsolidation behavior, the elasto-plastic constants used were the same values as used by Asaoka et al. 1994. Vertical constant loading rate was applied on the top surface. The boundary conditions were assumed to be constant lateral pressure and undrained conditions, with no friction at the top and bottom and with complete freedom of movement in the horizontal direction. Calculation under these conditions cannot be realized with quasi-static analysis that ignores inertial forces. The mesh subdivision was 70 elements laterally by 160 elements vertically.

Table 1 Specimen elasto-plastic constants and initial values

Elasto-plastic parameters	
Critical state index M	1.55
NCL intercept N	2.0
Compression index λ, ~	0.108
Swelling index κ, ~	0.025
Poisson's ratio ν	0.3
Evolution parameters	
Degradation index of OC m	0.2
Initial conditions	
Specific volume v_0	1.747
Stress ratio η_0	0.0
Degree of structure $1/R_0$ □	1.0
Degree of overconsolidation $1/R_0$	5.0
Degree of anisotropy ζ_0	0.0
Soil particle density ρ_s (g/cm^3)	2.65
Permeability coefficient k (cm/s)	3.7×10^{-8}

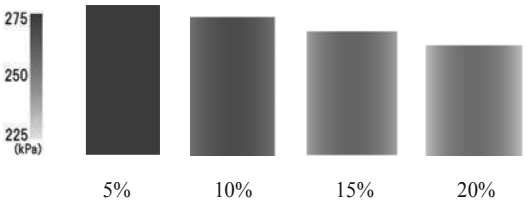

Fig. 2 Change in specimen deformation and pore water pressure distribution under uniform deformation

3 REPRODUCTION OF A UNIFORM FIELD USING THE GEOASIA ANALYSIS CODE

Consider undrained compression deformation of a perfectly rectangular specimen with no initial material or geometric imperfections. The top and bottom of the specimen were free in the horizontal direction, and after fixing the bottom in the vertical direction, a constant uniform vertical displacement was applied to the top. In accordance with the ***u-p*** Formulation, when solving without ignoring inertial forces, a uniform deformation field satisfying element-wise undrained conditions in a rectangular specimen can only be realized when the permeability coefficient is $k = 0$, although the theoretical proof (Noda et al. 2013) is omitted. In order to realize a uniform deformation field using this analysis code, it is necessary to set a velocity distribution that is proportional to the height and the velocity applied to the top of the specimen (not all are zero), an acceleration distribution to maintain the rectangular shape, and pore water pressures that exhibit a parabolic distribution in the horizontal direction as initial conditions in addition to the coordinates of the finite element nodes at the boundary and interior (Noda et al. 2013).

In this section, for the case with $k = 0$ first, a constant vertical velocity of 10^3 cm/s was applied on the top to illustrate the calculation results when a uniform deformation field is achieved. Fig. 2 shows the change in specimen deformation and the parabolic pore water pressure distribution, and Fig. 3 shows the horizontal component and vertical component of acceleration generated in the center of the right side surface of the specimen. However, when the theoretical initial values are set for the velocity and acceleration as initial conditions, small vibrations occur around time t=0. Therefore, for no vibration the initial velocities and accelerations are set slightly smaller than the theoretical values. See Noda et al. 2013 for the method of obtaining the reduced values.

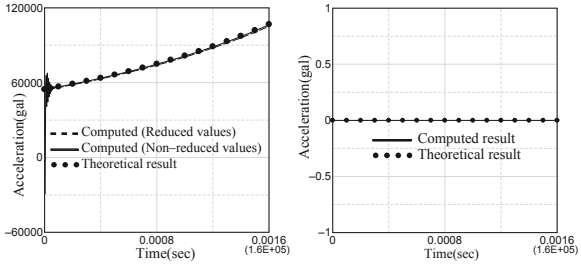

(i) horizontal (ii) vertical

Fig. 3 Difference in acceleration generated at the right side surface of the specimen

4 OCCURRENCE OF ACCELERATION ASSOCIATED WITH SHEAR BANDING

In the following, the initial conditions were changed from the conditions appropriate to realize a uniform deformation field to velocities, accelerations, and pore water pressures that are all zero. The calculation was carried out with (a) no initial geometric imperfections and (b) initial geometric imperfections applied to the specimen. In the case of (b), a half wavelength cosine curve (primary mode) with a small amplitude of 10^{-5} cm was applied to the side surfaces of the specimen in accordance with Asaoka et al. 1994. In static analysis, as in Asaoka et al. 1994, this is the shape of the induced initial imperfection, and it changed to the primary mode with reduction in load (imperfection-sensitive bifurcation behavior). In this section, in order for the specimen to maintain vertical symmetry in the case of (a), a vertical displacement at the constant rate of 0.5×10 cm/s was applied to both the top and bottom of the specimen in the compression direction. Also, the permeability coefficient was changed from zero to the values shown in Table 1. The calculation results are shown below.

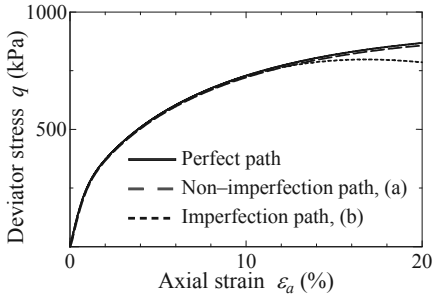

Fig. 4 Relationship between apparent q- ε_a with differences in initial imperfections

4.1 *VERTICALLY ASYMMETRIC DEFORMATION INDUCED BY INITIAL IMPERFECTIONS*

Fig. 4 shows the apparent axial differential stress q – axial strain ε_a relationship, and Fig. 5 shows the specimen shear strain distribution. q is the total increment of equivalent nodal forces obtained on the top divided by the area of the top at each time, and ε_a is the vertical displacement divided by the initial height. In the case of (a), q was virtually the same as the "perfect path" (= response of the constitutive equation) obtained in the uniform deformation field, and the specimen maintained left to right and top to bottom symmetry from the beginning to end. In contrast, in the case of (b), the deformation virtually maintained left to right and top to bottom symmetry up to an

ε_a of about 12%, but thereafter, vertical symmetry was broken. Associated with this deformation, q deviated from the perfect path and exhibited small values.

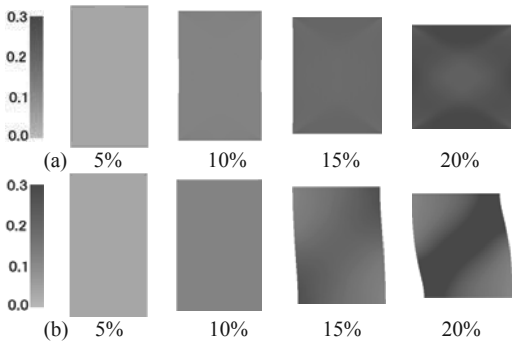

Fig. 5 Change in shear strain distribution in a specimen with initial imperfection in top loading
(a) No initial imperfections. (b) With initial imperfections.

4.2 *ACCELERATIONS ASSOCIATED WITH SHEAR BANDING AND THEIR FOURIER AMPLITUDES*

Fig. 6 shows the distribution of the horizontal component of acceleration generated in the specimen in (b). The acceleration distribution is symmetrical left to right and top to bottom up to about an ε_a of 12%. These are the accelerations generated due to the compression from the top and bottom as described above. In contrast, after the breakdown of vertical symmetry, localized

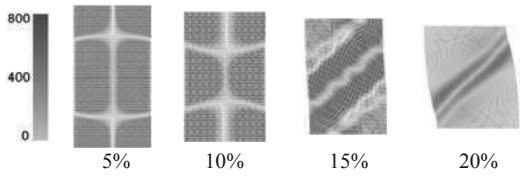

Fig. 6 Occurrence of shear banding associated with horizontal components of generated accelerations (gal)

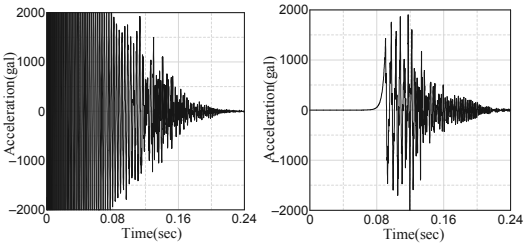

(i) Horizontal component (ii) Vertical component

Fig. 7 (i) Horizontal component and (ii) vertical component of acceleration generated at the side surface of the specimen

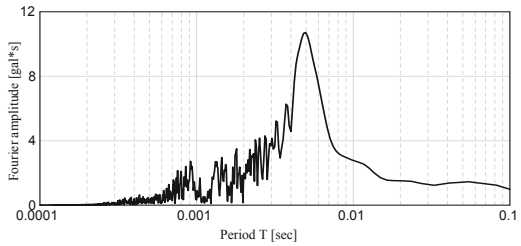

Fig. 8 Fourier amplitude of the vertical component of accelerations generated at point A

shear banding developed like reverse faults, and accelerations were generated along the shear bands. Fig. 7 shows (i) the horizontal component and (ii) the vertical component of acceleration generated at the node A shown in Fig. 1. Different from the horizontal component of acceleration, the vertical component was the component normal to the central axis of the specimen, and kept to be zero until about 0.08 sec after the start of loading, in other words, until the ε_a was about 10%. Thereafter, as the shear banding started, new accelerations were generated with a maximum value of about 2000 gal. Also, after exhibiting the maximum value of acceleration, each component tended to converge as ε_a increased. Fig. 8 shows the Fourier amplitude of the acceleration up to ε_a = 30% for the side surface (point A) of the specimen. From these figures, it can be seen that accelerations are generated predominantly with a period of around 5.0×10^{-3} sec.

5 LOADING RATE EFFECT

An investigation into the effect of displacement rate was carried out for compression under displacement control by applying a geometric initial imperfection in (b) of section 4. Fig. 9 shows the results of a comparison of the Fourier amplitudes of the accelerations obtained at point A on the side surface of the specimen for displacement velocities of 2.5 cm/s, 5 cm/s, and 10 cm/s. In all cases, the specimen deformed as in Fig. 5(b) (figures omitted). From Fig. 9, it can be seen that the Fourier amplitudes increase with velocity, as a loading rate effect, and that the predominant vibration amplitude is about 5.0×10^{-3} sec with almost no variation.

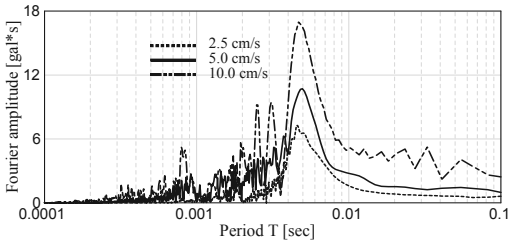

Fig. 9 Fourier amplitude of the vertical component of acceleration generated at point A on the right side surface of the specimen (load rate effect)

6 UNDRAINED CREEP BEHAVIOR UNDER CONSTANT LOAD

In this section, firstly all the initial and boundary conditions as well as the initial imperfection are same as (b) in section 4. The calculation performed was continued after deviation from the perfect path until (i) ε_a =13% (0.104 sec after the start) and (ii) ε_a =18.75% (0.150 sec after the start), and then was altered to load control at the top, maintaining the load constant, and continuing with displacement control on the bottom edge but stopping the vertical displacement. For load control, the conditions for the pedestal with no friction were calculated using the constraint conditions on the finite element nodes by the Lagrange method of undetermined multipliers, as in Asaoka et al. 1998. The results of the calculations are described below.

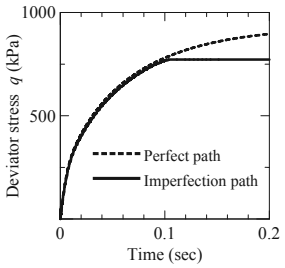

Fig. 10 Load control after displacement control ("creep")

Fig. 10 shows the relationship between the calculated specimen apparent top q and the elapsed time from displacement control, and Fig. 11 shows the change in axial strain from the start of displacement control. However, in Fig. 10, q was obtained by dividing by the initial area of the top of the specimen. Also, the ○ in Fig. 11 indicates the point of

change to load control. Figs. 12 and 13 show the vertical component of the velocity and acceleration, respectively, of the top of the specimen (in both cases, upwards is positive). In the case of both (i) and (ii), immediately after the change to load control, large changes in acceleration were seen, but in the case of (i), the changes soon converged. In contrast, in the case of (ii), after temporarily converging, the vertical velocity increased at around 0.5 sec to 0.9 sec in association with an increment in ac-

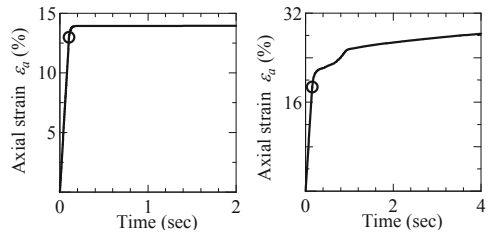

(i) 13% (ii) 18.75%

Fig. 11 Development of axial strain; ((i) and (ii) are the axial strain after changing to load control from displacement control)

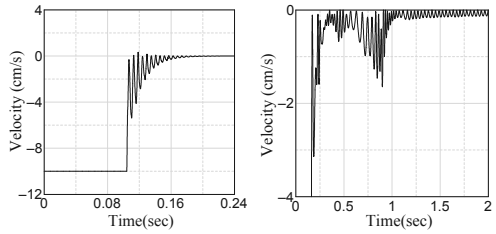

(i) 13% (ii) 18.75%

Fig. 12 Relationship between vertical velocity of the top and time

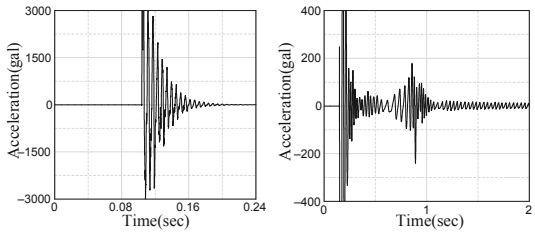

(i) 13% (ii) 18.75%

Fig. 13 Relationship between vertical acceleration of the top and time

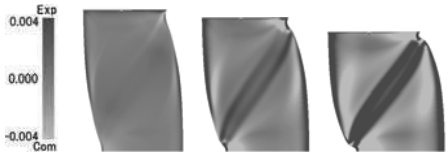

10% 28% 30%

Fig. 14 Changes in specific volume (swelling shear bands)

celeration and then reduced again, and thereafter, the axial strain slowly increased. In order to show the state occurring within the specimen at this time, Fig. 14 shows the change in specific volume within the specimen from the initial state. During the displacement control that included ε_a =10%, the loading was comparatively fast, so there was almost no migration of pore water within the specimen; however, under load control with the load constant, migration of pore water proceeded, causing flow into the shear band and swelling (generating swelling bands and acceleration).

7 CONCLUSION

This paper describes examples of calculation using the dynamic/static soil-water coupled finite deformation analysis code, GEOASIA in accordance with the ***u-p*** Formulation on the plane strain rectangular overconsolidated specimen under constant cell pressure and undrained conditions. The following is a summary of the new knowledge obtained:

1) Firstly, it was shown that a uniform deformation field in saturated soil under element-wise undrained conditions is possible when the permeability coefficient is zero, and that the output acceleration and pore water pressure field are in virtual agreement with the theoretical values. In order to realize this, it is necessary to apply a distribution of initially reduced velocities and accelerations, as well as pore water pressure within the specimen derived from theoretical considerations.

2) Next, initial velocity, acceleration, and pore water pressure values of zero were applied, and under vertical displacement control, vertical rates were applied with symmetric compression loading from the top and bottom. In this case, the lateral and vertical symmetry of the specimen broke down, and strain localization occurred. Also, in association with the occurrence of shear banding, when a vertical rate of 5 cm/s was applied, accelerations with a maximum of slightly less than 2000 gal were generated from the shear band with a predominant period of around 5.0×10^{-3} sec.

3) The load rate effect was investigated thirdly. The results showed that although the magnitudes of the Fourier amplitudes of the generated accelerations were different, the predominant period in all cases was unchanged at around 5.0×10^{-3} sec. Together with 2), in dynamic analyses, even though an acceleration time history such as input seismic motions, etc., has been applied to specimens or the ground, the point of view of generation of accelerations during the deformation of the soil or the ground itself has almost never been emphasized.

4) Finally, the specimen exhibited creep behavior under undrained conditions when the displacement control in 2) was changed to load control after the basic path deviated, and the load was maintained constant. When the load was held constant at a more unstable position, the axial displacement increased greatly with increases and decreases in acceleration in association with the development of shear bands associated with swelling (swelling bands). In this calculation, the inherent clay concept of the soil structure was not introduced, but it was shown that due to the existence of the inertia term and soil-water coupled behavior, large deformation associated with time dependence under load instability can be easily simulated.

8 REFERENCES

Ikeda, K. et al. 2003. Simulation and interpretation of diffuse mode bifurcation of elastoplastic solids, *J. Mech. Phys. Solids* 51 (9), 1649–1673.

Wan, R.G. et al. 1990. A Finite Element Method for the Analysis of Shear Bands in Geomaterials, *Finite Elem Anal Des* 7 (2), 129-143.

Asaoka, A. et al. 2007. All soils all states all round geo-analysis integration, *Implementation, Evaluation, and Application*, Hong Kong, China, 11-27.

Noda, T. et al. 2008. Soil-water coupled finite deformation analysis based on a rate-type equation of motion incorporating the SYS Cam-clay model, *S&F* 48 (6), 771-790.

Asaoka, A. et al. 2002. An elasto-plastic description of two distinct volume change mechanisms of soils, *S&F* 42 (5), 47-57.

Asaoka, A. et al. 1994. Imperfection-sensitive bifurcation of Cam-clay under plane strain compression with undrained boundaries, *S&F* 35 (1), 83-100.

Noda, T. et al. 2013. Realization of uniform deformation of soil specimen based on soil-water coupled finite deformation analysis considering inertia forces, *S&F*, to be submitted.

Asaoka, A. et al. 1998. Displacement/traction boundary conditions represented by constraint conditions on velocity field of soil, *S&F* 38 (4), 173-181.